Journal of Nuclear Materials 538 (2020) 152194

Contents lists available at ScienceDirect

Journal of Nuclear Materials

journal homepage: www.elsevier.com/locate/jnucmat

Modeling and simulation of oxygen transport in high burnup LWR fuel

Srdjan Simunovic [a, *], Theodore M. Besmann [b], Emily Moore [b, c], Max Poschmann [d], Markus H.A. Piro [d], Kevin T. Clarno [e], Jake W. McMurray [a], William A. Wieselquist [a]

[a] Oak Ridge National Laboratory, P.O. Box 2008-6085, Oak Ridge, TN, 37831, USA
[b] University of South Carolina, 541 Main St., Columbia, SC, 29208, USA
[c] Lawrence Livermore National Laboratory, L-372, 7000 East Ave., Livermore, CA, 94550, USA
[d] Ontario Tech University, 2000 Simcoe Street North, Oshawa, ON, L1G 0C5, Canada
[e] The University of Texas at Austin, 204 E. Dean Keeton St., Austin, TX, 78712-1591, USA

ARTICLE INFO

Article history:
Received 25 October 2019
Received in revised form
19 March 2020
Accepted 23 April 2020
Available online 3 June 2020

Keywords:
Nuclear fuel
Oxygen transport
Thermodynamics of nuclear fuel

ABSTRACT

We have developed a formulation for oxygen transport in uranium dioxide nuclear fuel that accounts for the effects of irradiation. The overall simulation combines the evolving isotopic composition, thermochemistry, and oxygen transport in irradiated fuel. The driving forces for oxygen transport are computed from local thermodynamic equilibrium calculations and account for the effects of temperature gradients and composition, including fission products. The proposed method provides a mechanism for including complex thermodynamic models of nuclear fuel in modeling of mass redistribution, and alleviates difficulties associated with the common thermodiffusion formulation. The transport model has been implemented within the nuclear fuel performance code BISON utilizing the thermochemistry code Thermochimica, with burnup calculations provided by the ORIGEN isotopic transmutation code.

1. Introduction

The evolving oxidation state and composition of Light Water Reactor (LWR) nuclear fuel has a strong influence on the performance and safety of reactor operation [1]. For instance, the temperature and oxygen chemical potential determine the chemical form of the fission products (e.g., whether they are stable as metals or oxides, dissolve in the fuel matrix, or form new phases, etc.), which in turn governs thermal conductivity, mechanical properties, etc. Characterization of the fuel composition during burnup has been presented in the literature [2–6] and will therefore not be reviewed in this document. The importance of simulating oxygen transport in the fuel under significant composition and large temperature gradients [7–15] is well understood, allowing the current paper to focus on describing model formulation and implementation.

A particular focus of this work is moving towards an approach that incorporates the effects of irradiation on the local oxygen chemical potential, where the gradient in oxygen potential drives its transport. As demonstrated by Piro et al. [16], the spatial variation of oxygen potential in irradiated fuel is affected by two competing, spatially varying factors: temperature and burnup. Temperature follows a parabolic profile with a minimum at the periphery and a maximum at the center, whereas burnup follows an exponential curvature with a minimum in the center and maximum at the periphery. Ultimately, the gradient in the oxygen potential changes at some point in burnup – not just due to temperature – which is a focus of this work. This effect cannot be accurately captured without incorporating fission products in the oxygen potential calculations. This paper is focused on better understanding and simulating the interaction of thermochemistry with mass transport to enable future engineering applications such as fuel failures under normal operating conditions, or assessing fuel integrity under disposal conditions.

Models for fuel behavior related to composition are usually derived from experiments on fresh fuel and – only in a very few instances – simulated irradiated fuel, which may rely on the assumption of a single UO_2 solid solution phase [17]. In reality, as the irradiation process progresses, multiple phases may form due to the creation of fission products from the consumed actinides and

* Corresponding author.
E-mail addresses: simunovics@ornl.gov (S. Simunovic), besmann@sc.edu (T.M. Besmann), moore236@llnl.gov (E. Moore), max.poschmann@ontariotechu.ca (M. Poschmann), markus.piro@ontariotechu.ca (M.H.A. Piro), clarno@utexas.edu (K.T. Clarno), mcmurrayjw1@ornl.gov (J.W. McMurray), wieselquiswa@ornl.gov (W.A. Wieselquist).

https://doi.org/10.1016/j.jnucmat.2020.152194
0022-3115/

their interactions with the fluorite-structure fuel phase. Thermochemical models predict the assemblage of stable phases at equilibrium and phase compositions that represent the lowest integral Gibbs energy for a given temperature, pressure, and composition [18–20]. These models are assumed to be good approximations of real phenomena because the high temperature of the fuel, random mixing nature of fission, and long time intervals at constant power/temperature drive the fuel to contain mesoscale volumes that quickly approach local thermodynamic equilibrium [21]. While thermodynamic equilibrium models by definition do not account for the kinetics of chemical processes that lead to the equilibrium state, they can provide the driving forces for kinetic models, such as those for oxygen transport.

The fission products and transuranics as solutes together with high temperatures and irradiation result in the formation of structural defects in the fluorite fuel phase. These defects in the UO_2 fluorite lattice control a wide range of phenomena in the fuel. The dominant structural defect is the formation of Frenkel defects on the oxygen anion sublattice [22]. Schottky defects are less prevalent and occur on both anion and cation sublattices. Oxygen transport occurs primarily through coordinated movement of defects on the anion lattice, whereas defect migration on the cation (i.e., uranium) sublattice requires substantially greater energies and thus occurs to a much smaller extent, but is significant enough to control the creep rate which is governed by movement of uranium vacancies.

Of primary interest here is the development of models for oxygen transport within the fluorite phase that depend upon composition and thermal gradients. In such a setting, diffusion is governed by more than just a concentration gradient. The diffusing species chemically interacts with the matrix and is influenced by variations in temperature and pressure. For the compositions and temperatures of interest, the fuel is essentially a single-phase fluorite-structured dioxide, and although minor noble metal phase inclusions are experimentally observed on the grain boundaries, no additional oxide phases have been experimentally observed within even highly irradiated LWR fuel with the possible exception at the very periphery of a fuel pellet. Thus, oxygen diffusion through only the single-phase material needs to be considered at this time.

In this work, we apply irreversible thermodynamics within a framework imposed by a Finite Element Method (FEM) description to formulate a computational model for oxygen transport in LWR fuel. Models for the mobility of oxygen in hypo- and hyper-stoichiometric nuclear fuel were adopted from the work by Moore et al. [23]. Temporally and spatially varying elemental composition as a function of burnup was calculated using the ORIGEN-S software [24]. The computed compositions were incorporated into the oxygen transport model and implemented in the BISON [25,26] fuel performance code. Thermochemical calculations were performed with Thermochimica [27], which was coupled to BISON.

2. Heat and species transport in chemical and temperature gradients

2.1. Transport model based on irreversible thermodynamics

Thermodynamic models determine the phase assemblage, phase compositions, and chemical potentials, and allow inference of the physical properties of a material system that is at thermodynamic equilibrium [28]. Thermodynamic equilibrium is defined as the minimum integral Gibbs energy state at constant temperature and pressure, with no entropy production and no unbalanced thermodynamic forces operating within the system. However, heat and species transport are irreversible, dissipative processes, driven by unbalanced driving forces. The processes considered here are assumed to occur over sufficiently large time intervals as to be treated as incrementally reaching steady-state [29]. The systems are open and thus energy and mass can be exchanged between a system and its surroundings. It is implicitly assumed that the system is sufficiently near equilibrium that there is a linear relationship between the driving forces and rate processes. These assumptions are not overly restrictive for diffusive transport, assuming that the gradients are not so large that they influence chemical reactions.

Heat and species transport simulations with chemical reactions are usually addressed using linear irreversible thermodynamics [30] based on the assumption of local equilibrium in the constitutive volumes, and conservation of energy and mass in the system. The macro non-equilibrium system is assumed to be an assembly of open equilibrated volume elements, and thus equilibrium thermodynamic relations are valid for locally defined thermodynamic variables. The elemental volumes can be used to describe heterogeneous systems as long as the temperature can be well-defined at every location. The intensive thermodynamic variables temperature (T), pressure (P), and chemical potential μ_k, of each component k, become functions of position vector $\boldsymbol{x}$, and time, t:

$$T = T(\boldsymbol{x}, t), P = P(\boldsymbol{x}, t), \mu_k = \mu_k(\boldsymbol{x}, t) \tag{1}$$

The extensive thermodynamic variables can be replaced by their volumetric densities

$$\overline{s} = \overline{s}(\boldsymbol{x}, t), \overline{h} = \overline{h}(\boldsymbol{x}, t), n_k = n_k(\boldsymbol{x}, t) \tag{2}$$

where $\overline{s}$, and $\overline{h}$, denote entropy and enthalpy per unit volume, and n_k denotes moles of component k per unit volume. Integrated values of the densities over the system volume do not mutually correlate by standard thermodynamic equilibrium relations because the overall system is not in equilibrium.

For spontaneous dissipative processes, entropy is produced in the system at a finite rate caused by the resistance against advancement of the underlying irreversible phenomena. The rate of the internal entropy production, σ, is used to identify and formulate fluxes and their conjugate driving forces. Alternatively, the quantity $T\sigma$, regarded as the rate of the dissipation of the Gibbs energy, $\dot{G}$, can be used to describe the changes in the properties of the system.

For the problem of simultaneous heat and mass transport, the internal entropy production rate density, σ, can be written in various forms using linear irreversible thermodynamics,

$$\sigma = J_q \cdot \nabla\left(\frac{1}{T}\right) - \sum_k J_k \cdot \nabla\left(\frac{\mu_k}{T}\right) \tag{3}$$

$$= J_q' \cdot \nabla\left(\frac{1}{T}\right) - \frac{1}{T}\sum_k J_k \cdot \nabla(\mu_k)_T \tag{4}$$

$$= TJ_s \cdot \nabla\left(\frac{1}{T}\right) - \frac{1}{T}\sum_k J_k \cdot \nabla\mu_k \tag{5}$$

where J_q, J_q', and (TJ_s), denote different definitions of the heat flux, and J_k denotes the flux of diffusing component k. The term $\nabla(\mu_k)_T$ denotes the gradient in chemical potential of component k while at constant temperature. In the heat flux definitions of Eqs. (3)–(5), one has:

$$J_q' = J_q - \sum_k h_k J_k \tag{6}$$

$$J_s = \frac{1}{T} J_q' + \sum_k s_k J_k \tag{7}$$

where J_q defines the total heat flux that includes pure heat conduction, J_q', and the effect of mass flux providing a partial specific enthalpy h_k. Similarly, J_s defines entropy flux that contains contributions from the heat conduction and the effect of mass flux providing a partial specific entropy s_k. Details regarding different heat flux definitions and the derivation of the above relations can be found in standard discussions of irreversible (non-equilibrium) thermodynamics [30,31]. The contribution of the local chemical reactions to the entropy production rate has not been included in Eqs. (3)–(5). We assume that the chemical reactions under the high temperatures of fissioning nuclear fuel are very fast and approach equilibrium, so that the corresponding driving forces and energy dissipation can be neglected [28]. The different forms of conjugate flux-force pairs in Eqs. (3)–(5) are equivalent, describing the same physical processes, and thus yield the same entropy production rate. Selection of the pairs is a matter of finding the most suitable and convenient formulation for describing the system.

In linear irreversible thermodynamics, the fluxes are linearly proportional to the driving forces, and the proportionality factors are phenomenological expressions that do not depend on the gradients of the thermodynamic variables. In the linear regime, the system converges to a stationary, steady-state with a constant entropy production rate. When fluxes are generalized to include coupling terms of the same dimensionality, proportionality coefficients L_{ij} are used to couple all the driving forces, F_j :

$$\begin{aligned} J_i &= \sum L_{ij} F_j \\ &= \mathbf{L} \cdot \mathbf{F} \end{aligned} \tag{8}$$

which form an Onsager coefficient matrix [32], **L**, and a vector of driving forces, **F**.

Conjugate pairs $\left(J_q', \nabla 1/T\right)$, and $\left(J_k, \nabla(\mu_k)_T\right)$ from Eq. (4) are most commonly used in the literature for modeling simultaneous heat and mass transport in solids. This approach is based on the assumption that we can separate the gradients of temperature and isothermal chemical potential as independent driving forces for heat flow and mass diffusion, respectively.

A number of coupled models for the transport of heat and oxygen in LWR fuel using thermodynamic driving forces have been reported [33–36]. These are based on the conjugate driving forces and fluxes of Eq. (4). The model parameters, such as thermodynamic factor and heat of transport, are often derived using the models of Lindemer and Besmann [17] for oxygen chemical potential or from experiments [37]. These models show the interplay between changing material composition and thermal properties, and oxygen and temperature distribution. An inherent difficulty with these models is separating of the driving force for oxygen flux into a driving force from the gradient of the isothermal chemical potential, and a driving force from the gradient of the temperature.

For the complex thermochemical phenomena and the corresponding thermodynamic models for fissioning nuclear fuel [18,21], the separation of the chemical potential driving forces using gradients of isothermal chemical potential and temperature,

$$\nabla \mu_k = \nabla(\mu_k)_T - s_k \nabla T \tag{9}$$

is not clearly defined nor practical. Ideally, we are looking for a set of equations that minimize or eliminate the cross terms $L_{ij,i\neq j}$ in Eq. (8) in order to simplify the formulation. In this work, we pursue the conjugate flux-force pairs from Eq. (5). We assume that the cross correlation of the selected thermodynamic forces is low, i.e. $L_{ij,i\neq j} = 0$, because the chemical potential gradient is the driving force for mass flux and includes the effects of both composition and temperature. We also assume that the heat flux in nuclear fuel is dominated by conduction, i.e., that the $\sum_k s_k J_k$ in Eq. (7) can be omitted. That contribution to the heat flow also vanishes when the diffusive driving force and mass flux vanish, i.e. when $J_k = 0$, and the oxygen distribution in the fuel reaches a steady state.

2.2. Transport model for component diffusion

Here we derive a constitutive model for the mass flux and mass conservation equations for modeling component diffusion in composition and temperature gradients. Using the volumetric density of a component, n_k, as a primary variable with units of $[\mathrm{mol}/\mathrm{m}^3]$, the mass flux is defined as the amount transported across a unit area normal to the flux direction per unit time. Assuming that the diffusing substance can be assigned an average constant drift velocity, v_k, its molar flux, J_k, is:

$$J_k = v_k n_k \tag{10}$$

where J_k has units of $[\mathrm{mol}/\mathrm{m}^2\mathrm{s}]$, and v_k has units of $[\mathrm{m}/\mathrm{s}]$. Using a linear approximation for uncorrelated movement of diffusing particles, the drift velocity is a result of the product of the driving force, F_k, imparted to a particle, and the proportionality factor, M_k:

$$v_k = M_k F_k \tag{11}$$

The proportionality factor M_k, termed mechanical mobility of substance k, is a reciprocal of the frictional drag experienced by a moving particle as it interacts with its environment. The mass flux-conjugate force from Eq. (5) that drives the system towards uniform thermodynamic potential for isobaric transport can be written as:

$$F_k = -\nabla \mu_k \tag{12}$$

which results in the flux:

$$J_k = -M_k n_k \nabla \mu_k \tag{13}$$

As noted in the previous section, for non-isothermal transport, the driving force is a gradient in chemical potential that embodies the effect of both composition and temperature. The mass conservation equation for implementation into an FEM solver can be written as:

$$\frac{\partial n_k}{\partial t} + \nabla \cdot \left(-M_k n_k \nabla \mu_{gk} \right) = 0 \tag{14}$$

The proposed formulation of Eq. (14) assumes transport occurs between infinitesimal volumes with uniform intensive variables. However, in the computational implementation, the values of the composition, temperature and chemical potential are interpolated in finite elements, and this interpolation allows us to compute the gradient of chemical potential within the element to allow the calculation of mass flux.

3. FEM implementation of the transport equations

We consider temperature distribution in the fuel pellet as an externally imposed field. Accordingly, the energy transport and balance equations are not used in the example models. Introduction of the fission heat generation, thermal transport, and accompanying material property variation into the model does not

present a fundamental difficulty and has been implemented by the authors for conventional transport models based on Eq. (4). However, for the purpose of illustration, adopting a fixed temperature field simplifies the calculations, presentation, and analysis of the results. Coupled transport models are currently under development for oxide and metal fuels and will be reported in the future.

Engineering transport models are based on spatial and temporal discretization of the domain of interest. They are usually cast in the form of control volumes and the integral form of conservation equations. The fuel performance code BISON [25] uses a Lagrangian FEM approach in which the weak form of conservation equations is solved. The FEM approach tracks the material volume, which is more suitable for mechanical and thermo-mechanical analyses of fuel performance.

To describe component transport using the relations of irreversible thermodynamics, the discretized form of Eq. (14) utilizes mass concentration of the diffusing component as the primary variable. It is based on local equilibrium within each sub-volume so that it can be described by local intensive variables, composition, and temperature. The FEM-discretized form commonly evaluates the intensive variables at the nodes of the FEM mesh, and their values are interpolated within finite elements using element interpolation functions. Thermochemical equilibrium and the resulting chemical potentials can be calculated within the finite elements using constant values of the intensive variables. They can also be evaluated at the nodes of finite elements, and their values interpolated within the elements.

The two forms of the discretized models are illustrated in Fig. 1. The two approaches to the non-isothermal mass diffusion are also described by Hillert [28], Sec. 5.6 and 5.7, respectively.

The discretization shown in Fig. 1a represents processes where each separate volume is at equilibrium for the given composition and temperature. The chemical potentials are thus at a minimum in each volume but values for individual components and temperature may be different between separate volumes. Even though each volume is at local equilibrium, a physical flux occurs to diminish the spatial difference in the Gibbs energy for the total volume. In this form, entropy production cannot occur in two adjacent volumes, but only between them, which requires boundary entropy production terms and partition of entropy between the two volumes [38].

In the continuum representation depicted in Fig. 1b, the volume element does not have to be at thermodynamic equilibrium. Temperature, composition, thermochemical equilibrium, and the corresponding chemical potentials are calculated at the finite element nodes, *i*. Their values are then interpolated as continuous variables across the element volume, so that their gradients (e.g., gradients of chemical potentials) are available within the volume. This form provides for continuity of intensive variables and thermodynamic functions. However, the interpolated variables, which are strictly defined only at equilibrium, may not have values that are consistent with the local equilibrium assumption. While recognizing this matter, when the equilibrium condition is enforced at the nodes, we consider the interpolated values of chemical potentials and other intensive variables within a volume to be sufficiently close to equilibrium. Accordingly, we adopted the continuum representation for implementing Eqs. (13) and (14). The composition and temperatures are defined at the nodes where the thermodynamic equilibrium and the chemical potentials are evaluated. Consequently, the gradient of the chemical potential is evaluated at the integration points of the finite elements for mass flux and integration calculation purposes.

The integral form of the mass conservation equation for implementation in the FEM framework is:

$$\int_V \frac{\partial n_k}{\partial t}\psi dV - \int_V J_k \nabla\psi dV + \int_\Gamma \psi J_k \cdot \hat{n} d\Gamma = 0 \tag{15}$$

where V and Γ are the volume and surface of the domain, respectively, ψ denotes the test functions, and $\hat{n}$ is the outward normal vector to the domain surface.

In more compact notation, as used in the Multiphysics Object-Oriented Simulation Environment (MOOSE) [39], which is the underlying FEM framework for the nuclear fuel performance code BISON, the integral equation (Eq. (15)) is written as:

$$R(c_k) = \left(\frac{\partial n_k}{\partial t}, \psi\right) - (\nabla\psi, J_k) + \langle \psi, J_k \cdot \hat{n}\rangle = 0 \tag{16}$$

where parentheses and angle brackets denote corresponding inner products integrated across the domain and over its surface, respectively. The concentration field, n_k, at any location is represented by values at the nodes of a finite element mesh, n_{kj}, and their nodal shape functions, φ_j, such that:

$$n_k = \sum_j n_{kj}\varphi_j \tag{17}$$

In the FEM formulation used in MOOSE, the test and shape functions are the same. Using Eq. (17), the residual of Eq. (16) is a vector $\boldsymbol{R}(\boldsymbol{n_k})$ of the nodal values, $\boldsymbol{n_k}$, and the resulting system of nonlinear equations can be solved using Newton's method by iteratively driving the residual vector to zero. The components of the residual vector are:

$$R_i(\boldsymbol{n_k}) = \left(\frac{\partial \boldsymbol{n_k}}{\partial t}, \psi_i\right) - (\nabla\psi_i, J_k) + \langle \psi_i, J_k \cdot \hat{n}\rangle, i = 1, .., N \tag{18}$$

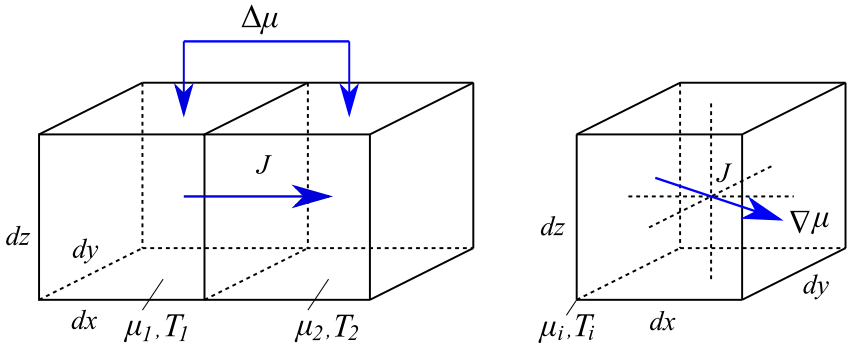

Fig. 1. Volume elements for (a) discontinuous adjacent volumes in local equilibrium, and for (b) a continuum representation [38].

where index i denotes the finite element mesh node index associated with the test function ψ_i , and N denotes the number of FEM nodes. The elements of the Jacobian matrix, $\mathcal{J}_{ij}$, required for the Newton iterations are:

$$\mathcal{J}_{ij}(\boldsymbol{n_k}) = \frac{\partial R_i(\boldsymbol{n_k})}{\partial n_{kj}} \tag{19}$$

where indices i and j denote nodes in the FEM mesh, and n_{kj} denotes a value of $\boldsymbol{n_k}$ at node j. The inner products in Eq. (18) involve derivatives of the mass flux with respect to concentration at node j:

$$\left(\nabla\psi_i, \frac{\partial J_k}{\partial n_{kj}}\right), \langle \psi_i, \frac{\partial J_k}{\partial n_{kj}} \cdot \hat{n}\rangle \tag{20}$$

and refer to derivatives of the mass flux in equation for J_k. In MOOSE Jacobian-free Newton Krylov (JFNK) solver, an approximate expression for the Jacobian is, nevertheless, necessary in order to achieve a reasonable convergence rate. Using

$$\frac{\partial \boldsymbol{n_k}}{\partial n_{kj}} = \sum_i \frac{\partial}{\partial n_{kj}}(n_{ki}\varphi_i) = \varphi_j \tag{21}$$

for the mass flux in Eq. (16), the Jacobian inner product terms can be approximated as:

$$(\nabla\psi_i, -M_k F_k \varphi_j), \langle \psi_i, -M_k F_k \varphi_j \cdot \hat{n}\rangle \tag{22}$$

which omits the partial derivatives of $-M_k$ and F_k.

The thermodynamic solver Thermochimica computes values of the chemical potential at the nodes, however, their partial derivatives that would be required for Jacobian terms of F_k are not readily available and would be expensive to calculate through numerical differentiation. Using an ideal solution approximation for the oxygen chemical potential for calculating the Jacobian of its gradient has not been productive, perhaps due to the opposite direction of this approximation compared to the gradient of the original potential. We are currently investigating different approaches for deriving better Jacobian approximations and will report on the progress in future publications.

4. Computing local fuel composition with burnup

The composition of nuclear fuel evolves during burnup as actinides are consumed during fission and additional chemical elements are created through depletion, decay, and transmutation. Thus, it is important to account for the effects of changing elemental composition on oxygen transport. Details of nuclear fuel burnup described by Walker et al. [3] and modeled by Piro et al. [16,40] were used in example calculations in the current work. The elemental composition along the radius of the pellet as a function of time was calculated using the ORIGEN-S depletion code [24] and supplied to the nuclear fuel performance code BISON as a function of time and space. Oxygen was the only component permitted to be transported in this simulation. While this is clearly not entirely consistent with what happens in real fuel, which would involve fission product transport, the intent here is to focus on a mechanistic approach to mass transport simulations by thermodynamically informed coupling.

5. Thermodynamic model for LWR fuel

The thermodynamic model used to represent $UO_{2\pm x}$ in this analysis is based on that of Guéneau et al. [20]. This model represents the fluorite phase using a Compound Energy Formalism (CEF) [41] approach with three sublattices. The first sublattice represents the normal cationic site (U^{3+}, U^{4+}, U^{5+}), the second sublattice represents the normal anionic site (O^{2-}, Va), and the third sublattice represents the interstitial site (O^{2-},Va), where Va indicates a lattice site vacancy. This particular model reproduces the phase equilibria for the U–O system quite well in addition to allowing accurate oxygen potential calculations. Fig. 2 shows the U–O phase diagram calculated by Thermochimica using this thermodynamic model with oxygen partial pressure isobars superimposed.

While it is possible to obtain all produced elements from the depletion calculations, it is useful to limit consideration to generated elements present at greater than trace amounts. In addition, thermodynamic values and models for phases that can form from all of the remaining elements are not available. To address that issue, the elements lacking phase information were aggregated with those displaying similar chemical behavior as indicated in Table 1.

To include the significant number of additional elements in equilibrium calculations for the fuel compositions requires a more extensive thermodynamic model of the fluorite fuel phase beyond just the U–O system. This has been accomplished utilizing an expansion of the approach of Guéneau et al. [20] with the fluorite phase represented by the CEF model of Besmann et al. [18] with the three sublattices defined as

$$\begin{gathered}\left(U^{+3,4,5,6}, Pu^{+3,4}, Y^{+3}, Nd^{+3}, La^{+3}, Pr^{+3,4}, Ce^{+3,4}, Te^{+4}, Mo^{+4}, Zr^{+2,4}\right)_1 \\ \left(O^{-2}, Va\right)_2 \left(O^{-2}, Va\right)_1\end{gathered} \tag{23}$$

From an equilibrium thermodynamic point of view, there is also the possibility of formation of secondary phases, many of which can have variable cationic composition (solid solution) as does the fluorite phase. One of the most likely is the complex perovskite forming from among the higher concentration fission product elements. Its thermodynamic description was obtained from the Thermodynamics for Advanced Fuels-International Database (TAF-ID) [43,44], which utilizes a three sublattice CEF model as follows

$$\left(Ba^{2+}, Ca^{2+}, Sr^{2+}\right)\left(Ba^{2+}, U^{4+}, Mo^{4+}, U^{6+}, Zr^{4+}\right)\left(O^{2-}\right)_3 \tag{24}$$

Additional phases included $(Rb, Cs)_2UO_4$, $(Rb, Cs)MoO_4$, and $(Rb, Cs)_2ZrO_3$ modeled as ideal solutions of the relevant pseudo-binary oxide phases using thermodynamic values obtained from the FactPS database of the FactSage [45] thermochemical software suite. The remaining phases also considered in equilibrium calculations are described by Besmann et al. [18].

6. Demonstration problems

Two demonstration problems are presented, both of which

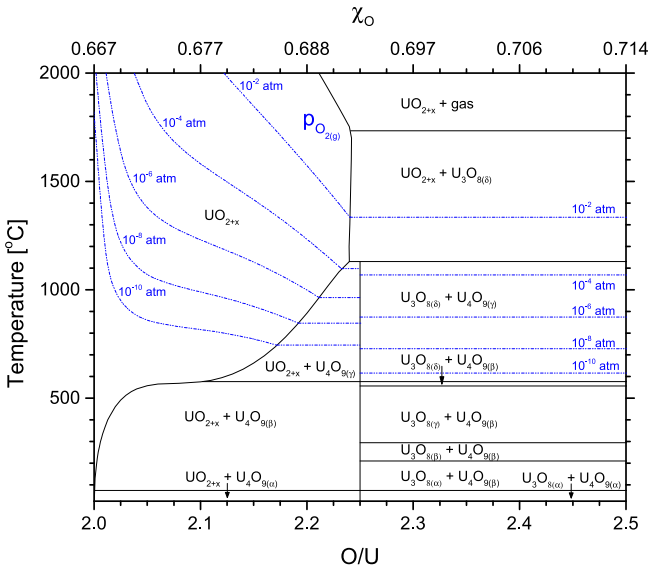

Fig. 2. A binary phase diagram of the U–O system used in this work is shown with partial pressures of oxygen superimposed [42].

Table 1
Aggregated elements used in equilibrium calculations.

Aggregated element	Included element
Pu	Am, Np
Zr	Nb
Nd	Pm, Sm, Eu
Ba	Sr
Te	Se

simulate oxygen transport in $UO_{2\pm x}$ fuel with a prescribed temperature field. An axisymmetric model of a radial section of a fuel pellet from Walker et al. [3] was used for the simulation of oxygen transport during irradiation. The pellet diameter was 9.3 mm and a parabolic temperature profile was imposed with a fuel centerline temperature of 1873 K and fuel pellet surface temperature 835 K. The parabolic temperature profile (shown in Fig. 3) simulates the effects of a volumetric heat source possessing a low thermal conductivity. In both cases, the initial fuel composition is taken to be uniform $UO_{2.005}$. In the first demonstration problem, the total composition is not modified, and all local compositional changes within the fuel element are due to the diffusion of oxygen as described by Eq. (14). In the second demonstration problem, the fuel composition at each point in the system evolves over time due to burnup (as calculated by Piro et al. [16]) as well as due to oxygen diffusion.

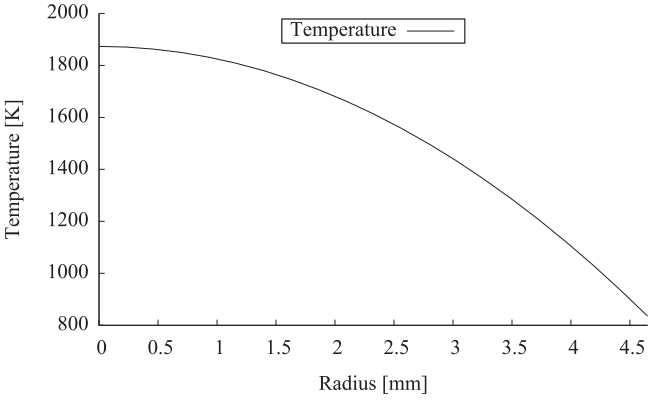

Fig. 3. Temperature distribution along the pellet radius.

In $UO_{2\pm x}$ fuel, the three main types of oxygen transport are by interstitial diffusion (in hyper-stoichiometric fuel, UO_{2+x}), vacancy diffusion (in hypo-stoichiometric fuel, UO_{2-x}) [23], and gas phase transport. The first two mechanisms are captured in the model presented. We use the mobility model for non-stoichiometric $UO_{2\pm x}$ from Moore et al. [23], obtaining M_k for Eq. (14). In this model, the mobility of O (M_O) is taken to be the sum of the mobilities of O interstitials (M_i) and O vacancies (M_{Va}). In turn, these are:

$$M_i = y_i(1-y_i)M_i^0 \exp\left(\frac{-Q_i + y_i(1-y_i)A_i}{RT}\right) \tag{25}$$

$$M_{Va} = y_{Va}(1-y_{Va})M_{Va}^0 \exp\left(\frac{-Q_{Va} + y_{Va}(1-y_{Va})(A_{Va}-BT)}{RT}\right) \tag{26}$$

where y_i is the site fraction of O interstitials, y_{Va} is the site fraction of oxygen vacancies, and the mobility parameters were taken to be those in Table 2, from Fig. 6 in Ref. [23].

In the case of interstitial diffusion, solute oxygen anions move among interstitial oxygen sites in the host UO_2 lattice. The defects that facilitate transport are controlled by stoichiometry and, in the case of interstitial diffusion, the movement is not accompanied by a counter-movement of a defect, such as a vacancy. If the underlying intrinsic mechanism of transport and the mobility for each thermodynamic driving force is the same, then such an interpolation can be further simplified by the use of a common mobility factor. Where the concentration of the moving substance is given as a fraction of its total amount, such as the site fraction of interstitial oxygen, y_{iO}, in UO_{2+x}, the flux in Eq. (13) has to be accordingly scaled by the same factor.

6.1. Oxygen transport in $UO_{2.005}$ under a temperature gradient

In this example, only the effects of the imposed temperature gradient and time on the oxygen transport problem are demonstrated. Diffusion was allowed to take place for up to one year, while no other changes to the state of the system were made. Figures 4–5 show the oxygen-to-uranium ratio and oxygen chemical potential along the radius of the pellet during this period. Thin gray lines between the beginning and end states denote distributions at one month increments. Note that the CEF thermodynamic model for UO_{2+x} of Guéneau et al. [20] used here reflects the understanding that the energetics cause the formation of oxygen site defects to be many times more likely than equivalent uranium site defects, and they were therefore not considered in the model. In addition, the model yields a negligible amount of disorder with respect to oxygen normal and interstitial lattice sites, that is, there are vanishingly few normal oxygen site vacancies compensated by oxygen interstitials. The exception is at extremely high temperatures, well above those considered here. Thus, as oxygen interstitials are essentially the sole cause of the hyperstoichiometry in UO_{2+x}, the value of the molar number of oxygen interstitial defects per mole of UO_{2+x} is simply equal to x.

This simulation shows transport of oxygen down the chemical potential gradient (up the temperature gradient) toward the more negative chemical potential, entirely driven by the temperature gradient. After one year, the oxygen chemical potential has become nearly uniform across the pellet as would be the case for a closed system at equilibrium, which requires the chemical potential of each component to be uniform across the material. The exception is

Table 2
Oxygen mobility parameters [23].

Regular Sublattice (M_{Va})		Interstitial Sublattice (M_i)		Units
Q_{Va}	53498	Q_i	95411	[J/mol]
M^0_{Va}	4.38×10^{-12}	M^0_i	2.76×10^{-10}	[(mol·m^2)/(J·s)]
$A_{Va} - BT$	$2234 - 19.91T$	A_i	-90548	[J/mol]

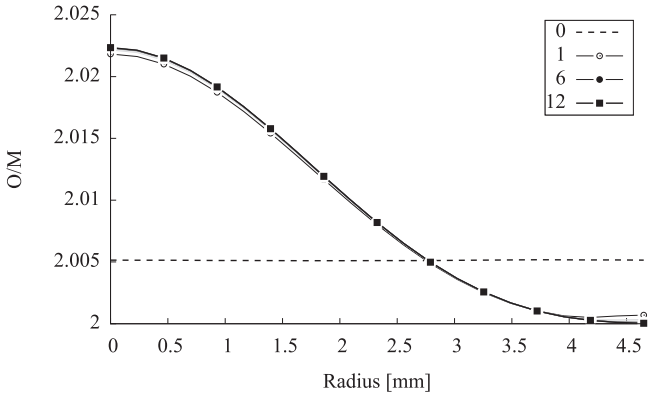

Fig. 4. Evolution of the oxygen-to-uranium ratio along the pellet radius. No fission products were considered. The numbers in the legend refer to months in-reactor.

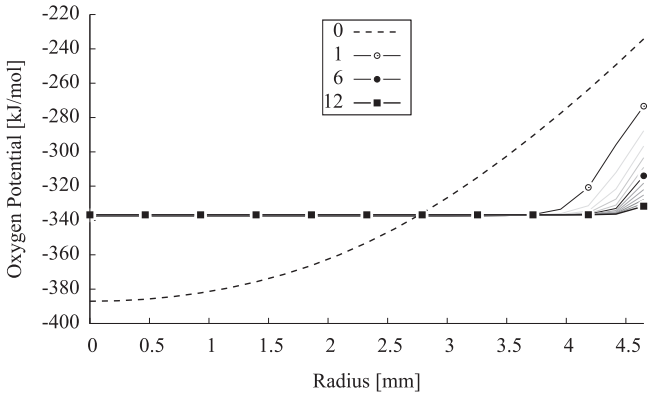

Fig. 5. Evolution of oxygen chemical potential along the pellet radius. No fission products were considered. The numbers in the legend refer to months in-reactor.

the pellet periphery where the mobility of oxygen is slow due to the relatively low temperature.

6.2. Oxygen transport under a temperature gradient as a function of burnup

As in the previous example, the duration of the second demonstration simulation was only one year as the purpose was to demonstrate the capability of the formulation. The equivalent composition at that time is shown in Fig. 6. In the simulation, the fission product inventory is read into BISON as a function of time and position, and BISON provides the composition information to Thermochimica when equilibrium thermochemical calculations are required.

Figure 7 shows the oxygen to metal ratio in the fluorite phase after one year of burnup. Here, some fission products have different oxidation states from that of uranium and there is also a loss of uranium to fission or neutron absorption/decay. The net effect is that the oxygen to metal ratio is generally lower than in the simulation without burnup.

Figure 8 shows the oxygen chemical potential along the radius of the pellet up to one year of burnup. The results are largely similar to those before irradiation as the oxygen chemical potential seeks to become uniform across the radius again, not approaching equilibrium at the periphery due to lower oxygen mobility.

7. Discussion and potential future work

Multi-physics simulations presented in this work that coupled thermodynamic calculations from Thermochimica directly with oxygen diffusion calculations in BISON demonstrated intuitively correct results for two demonstration problems in the previous section. The first considered fresh fuel, whereby the oxygen potential was only affected by temperature, which drives oxygen to diffuse up the temperature gradient. This is to be expected and is consistent with many other simulations reported in the open literature. The second demonstration problem was unique in that fission products were included in the simulation, which affected the calculation of the oxygen chemical potential, thereby having an impact on the diffusion of oxygen by accounting for the effects of irradiation in thermochemical calculations.

While this particular simulation imposed a fixed parabolic temperature distribution to focus the attention on thermochemistry and thermodiffusion coupling, other physical phenomena pertinent to fuel performance can be fairly easily added as they are already available in BISON. The current work was focused on fundamental capability development, and will be subsequently shifting to engineering applications.

A pertinent application of the aforementioned computational framework, including some future anticipated developments, is to predict the likelihood of fuel failure. One particularly important failure mechanism is Pellet Cladding Interaction (PCI), that can include Stress Corrosion Cracking (SCC) in the cladding assisted by chemical attack by volatile fission products (notably iodine) [46]. Some experiments in research and test reactors have indicated that oxide on the inner surface of the cladding can afford sufficient protection against SCC by providing a passivation layer [46]. Also, Arimescu and Karlsson [47] have reported findings from the Studsvik Cladding Integrity Project (SCIP-III) that suggest that slow power ramps are beneficial to PCI mitigation where the slow ramp provides sufficient time for an oxide passivation layer to form on the inner cladding surface to protect it from SCC.

The computational framework described herein would provide a tool to explore the effects of irradiated fuel chemistry and the role of oxygen transport on SCC susceptibility, among other practical fuel failure mechanisms. This may include simulating the redistribution of oxygen in different fuel designs with various dopants (e.g., Cr_2O_3, Al_2O_3–Cr_2O_3, Gd_2O_2, etc.), and even extend to transport of reactive fission products to the cladding inner surface, to support fuel integrity analyses.

Very good progress has been made by Konarski et al. [35] with the ALCYONE code in simulating fuel performance for practical engineering applications, including PCI susceptibility. In their work, thermochemical calculations enabled the inclusion of chromia

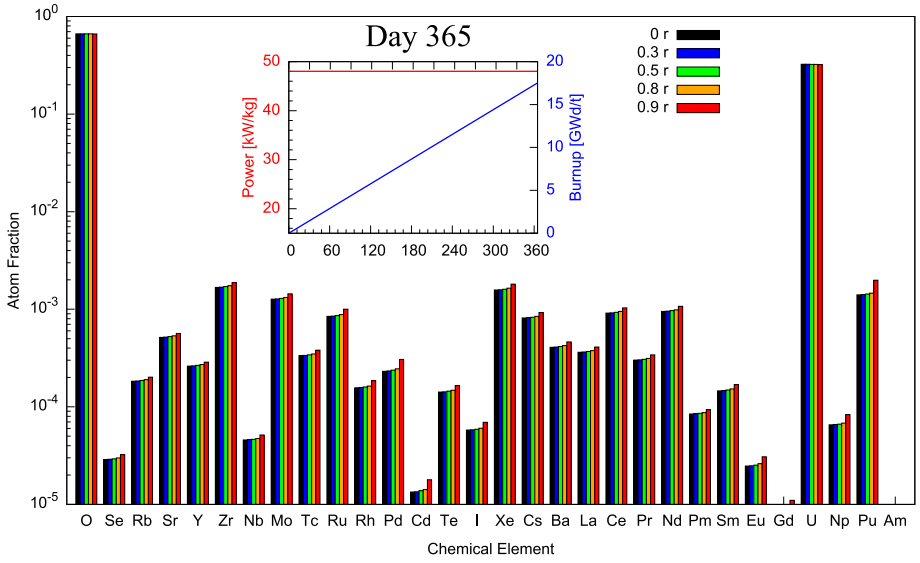

Fig. 6. Simulated elemental composition after 365 days.

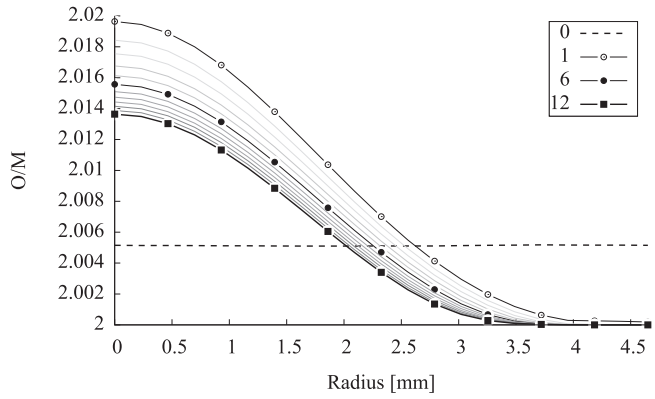

Fig. 7. Evolution of the oxygen-to-metal ratio in the fluorite fuel phase along pellet radius. Fission products were considered. The numbers in the legend refer to months in-reactor.

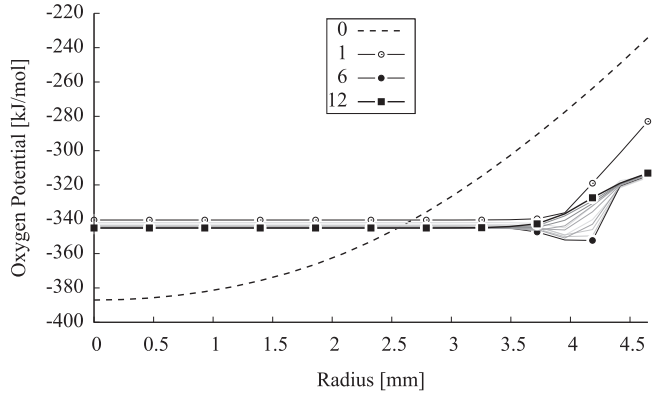

Fig. 8. Evolution of oxygen chemical potential along the pellet radius. Fission products were considered. The numbers in the legend refer to months in-reactor.

dopants. The code also has sophisticated methods of capturing pellet fracture, which is another important factor to consider in PCI behaviour. The work of Konarski et al. [35] differs from the current work in that the former used the semi-empirical approach based on concentration gradients, which proves challenging when trying to capture the effects of irradiation on thermochemistry.

The approach using the described code configuration in BISON has been computationally expensive to use because the thermodynamic equilibrium calculations require nested, iterative Gibbs energy minimization calculations at every computation point in space with multiple iterations per timestep. To at least partially address that problem, new algorithms for improving the solver performance were developed, which make Thermochimica much more computationally affordable for fuel performance modeling [48]. These performance enhancements operate by making use of values computed by Thermochimica from a previous time step as initial estimates of stable phases and species concentrations for the subsequent time step. Previously, every call to Thermochimica would start anew without any prior knowledge of the system. Clearly, this is a more intuitive way to couple thermodynamic calculations with multi-physics calculations, which have provided performance improvements upwards of a factor of five in coupled BISON-Thermochimica calculations.

8. Summary

We have developed a formulation for oxygen transport in oxide nuclear fuels with compositional and temperature non-uniformity that represents energetics-driven redistribution in a mechanistic fashion. The proposed model for oxygen transport is based on the full gradient of the oxygen chemical potential that is evaluated at the nodal points of the FEM mesh of the transport model. The formulation was demonstrated on the problem of temporally and spatially varying radial composition of a nuclear fuel pellet undergoing burnup.

The significant difference in oxygen diffusion between the example problems of an unirradiated, uniform composition $UO_{2.005}$ fuel pellet and that of irradiated fuel with position-dependent burnup and a substantial fission product inventory, demonstrates the importance of performing detailed thermochemical calculations. The calculations yielded apparent variations in oxygen diffusion rate, oxygen concentration profile, and average oxidation state in the fluoride phase during the one year simulation considered. In addition to being important for simulating conventional oxide fuel behavior, the thermochemical models will also be

important in accurately predicting the effects of various additives currently being considered for advanced fuels. Optimizing our strategy for defining material composition and improving the efficiency of thermodynamics calculations present additional opportunities for improving modeling capability.

Notice

Declaration of competing interest

The authors declare that they have no known competing financial interests or personal relationships that could have appeared to influence the work reported in this paper.

CRediT authorship contribution statement

Srdjan Simunovic: Conceptualization, Methodology, Software, Writing - original draft. **Theodore M. Besmann:** Conceptualization, Methodology, Writing - original draft. **Emily Moore:** Methodology. **Max Poschmann:** Conceptualization, Methodology, Software, Writing - original draft. **Markus H.A. Piro:** Conceptualization, Methodology, Software, Writing - original draft. **Kevin T. Clarno:** Software. **Jake W. McMurray:** Methodology. **William A. Wieselquist:** Software.

Acknowledgements

M.H.A. Piro thanks M.J. Welland (CNL) for many years of fruitful discussions on bridging classical thermodynamics and kinetics. Also, technical discussions with J. Sercombe (CEA) on PCI behaviour and fuel performance code are greatly appreciated.

Research was sponsored by the U.S. Department of Energy, Office of Nuclear Energy, Nuclear Energy Advanced Modeling and Simulation Program and Fuel Cycle R&D Program, under contract DE-AC05-00OR22725 with UT-Battelle, LLC.

This research was undertaken, in part, thanks to funding from the Canada Research Chairs program (950−231328) of the Natural Sciences and Engineering Research Council of Canada.

References

[1] D.R. Olander, Fundamental Aspects of Nuclear Reactor Fuel Elements, Technical Information Center, Office of Public Affairs, Energy Research and Development Administration, 1976.
[2] D.R. Olander, Mechanistic interpretations of UO_2 oxidation, J. Nucl. Mater. 252 (1−2) (1998) 121−130, https://doi.org/10.1016/s0022-3115(97)00291-2.
[3] C.T. Walker, V.V. Rondinella, D. Papaioannou, S. Van Winckel, W. Goll, R. Manzel, On the oxidation state of UO_2 nuclear fuel at a burn-up of around 100 MWd/kgHM, J. Nucl. Mater. 345 (2−3) (2005) 192−205, https://doi.org/10.1016/j.jnucmat.2005.05.010.
[4] K. Park, M.S. Yang, H.S. Park, The stoichiometry and the oxygen potential change of urania fuels during irradiation, J. Nucl. Mater. 247 (1997) 116−120, https://doi.org/10.1016/s0022-3115(97)00068-8.
[5] R.J. Konings, Comprehensive Nuclear Materials, Elsevier Science, 2012.
[6] C. Guéneau, J.-C. Dumas, M. Piro, In-reactor behavior, in: M. Piro (Ed.), Advances in Nuclear Fuel Chemistry, Elsevier, 2020, pp. 419−468, book section 11.
[7] D. Marchant, H. Bowen, Oxygen redistribution in UO_2 due to a temperature gradient, in: A. Cooper, A. Heuer (Eds.), Mass Transport Phenomena in Ceramics, vol. 9, Springer, 1975, pp. 97−109.
[8] M.G. Adamson, E.A. Aitken, S.K. Evans, J.H. Davies, Oxygen redistribution and its measurement in irradiated oxide fuels. Thermodynamics of Nuclear Materials 1974, 1975, pp. 59−71. Vienna, Austria.
[9] M.G. Adamson, R.F.A. Carney, Mechanistic study of oxygen thermal-diffusion in hyperstoichiometric urania and urania-plutonia solid-solutions, J. Nucl. Mater. 54 (1) (1974) 121−137, https://doi.org/10.1016/0022-3115(74)90083-x.
[10] S.K. Evans, E.A. Aitken, C.N. Craig, Effect of a temperature gradient on stoichiometry of urania-plutonia fuel, J. Nucl. Mater. 30 (1−2) (1969) 57−61, https://doi.org/10.1016/0022-3115(69)90168-8.
[11] J.F. Marin, P. Contamin, Uranium and oxygen self-diffusion in UO_2, J. Nucl. Mater. 30 (1−2) (1969) 16−25, https://doi.org/10.1016/0022-3115(69)90164-0.
[12] J. Janek, H. Timm, Thermal diffusion and Soret effect in $(U,Me)O_{2+\delta}$: the heat of transport of oxygen, J. Nucl. Mater. 255 (2−3) (1998) 116−127, https://doi.org/10.1016/s0022-3115(98)00037-3.
[13] K. Lassmann, The oxired model for redistribution of oxygen in non-stoichiometric uranium plutonium oxides, J. Nucl. Mater. 150 (1) (1987) 10−16, https://doi.org/10.1016/0022-3115(87)90088-2.
[14] D.R. Olander, Oxygen redistribution in UO_{2+x}, J. Nucl. Mater. 44 (1) (1971) 116−120, https://doi.org/10.1016/0022-3115(72)90140-7.
[15] H. Matzke, Atomic transport-properties in UO_2 and mixed oxides $(U,Pu)O_2$, J. Chem. Soc. Faraday Trans. II 83 (1987) 1121−1142, https://doi.org/10.1039/f29878301121.
[16] M. Piro, J. Banfield, K. Clarno, S. Simunovic, T. Besmann, B. Lewis, W. Thompson, Coupled thermochemical, isotopic evolution and heat transfer simulations in highly irradiated UO_2 nuclear fuel, J. Nucl. Mater. 441 (1−3) (2013) 240−251, https://doi.org/10.1016/j.jnucmat.2013.05.060.
[17] T.B. Lindemer, T.M. Besmann, Chemical thermodynamic representation of UO_{2+x}, J. Nucl. Mater. 130 (Feb) (1985) 473−488, https://doi.org/10.1016/0022-3115(85)90334-4.
[18] T.M. Besmann, J.W. McMurray, S. Simunovic, Application of thermochemical modeling to assessment/evaluation of nuclear fuel behavior, Calphad Comput. Coupling Phase Diagrams Thermochem. 55 (2016) 47−51, https://doi.org/10.1016/j.calphad.2016.04.004.
[19] C. Guéneau, M. Baichi, D. Labroche, C. Chatillon, B. Sundman, Thermodynamic assessment of the uranium-oxygen system, J. Nucl. Mater. 304 (2−3) (2002) 161−175, https://doi.org/10.1016/s0022-3115(02)00878-4.
[20] C. Guéneau, N. Dupin, B. Sundman, C. Martial, J.C. Dumas, S. Gossé, S. Chatain, F. De Bruycker, D. Manara, R.J.M. Konings, Thermodynamic modelling of advanced oxide and carbide nuclear fuels: description of the U-Pu-O-C systems, J. Nucl. Mater. 419 (1−3) (2011) 145−167, https://doi.org/10.1016/j.jnucmat.2011.07.033.
[21] T.M. Besmann, Computational thermodynamics: application to nuclear materials, in: R.J. Konings (Ed.), Comprehensive Nuclear Materials, 1, Elsevier, 2012, pp. 455−470, book section 1.17.
[22] H. Matzke, Diffusion in nonstoichiometric oxides, in: T. Sorensen (Ed.), Non-stoichiometric Oxides, Academic Press, 1981, pp. 155−269, book section 4.
[23] E. Moore, C. Guéneau, J.-P. Crocombette, Diffusion model of the non-stoichiometric uranium dioxide, J. Solid State Chem. 203 (2013) 145−153, https://doi.org/10.1016/j.jssc.2013.04.006.
[24] I. Gauld, O. Hermann, R. Westfall, ORIGEN SCALE System Module to Calculate Fuel Depletion, Actinide Transmutation, Fission Product Buildup and Decay, and Associated Radiation Terms, Report ORNL/TM-2005/39, Oak Ridge National Laboratory, 2005.
[25] J.D. Hales, S.R. Novascone, B.W. Spencer, R.L. Williamson, G. Pastore, D.M. Perez, Verification of the BISON fuel performance code, Ann. Nucl. Energy 71 (2014) 81−90, https://doi.org/10.1016/j.anucene.2014.03.027.
[26] Idaho National Laboratory, BISON: A Finite Element-Based Nuclear Fuel Performance Code, 2020. https://bison.inl.gov.
[27] M. Piro, S. Simunovic, T. Besmann, B. Lewis, W. Thompson, The thermochemistry library Thermochimica, Comput. Mater. Sci. 67 (2013) 266−272, https://doi.org/10.1016/j.commatsci.2012.09.011.
[28] M. Hillert, Phase Equilibria, Phase Diagrams and Phase Transformations, Their Thermodynamic Basis, second ed., Cambridge University Press, New York, 2007.
[29] N.W. Tschoegl, Fundamentals of Equilibrium and Steady-State Thermodynamics, Elsevier Science & Technology Books, 2000.
[30] S. de Groot, P. Mazur, Non-Equilibrium Thermodynamics, Dover Publications, Inc., 2011.
[31] S. Kjelstrup, D. Bedeaux, Non-Equilibrium Thermodynamics of Heterogeneous Systems, World Scientific, 2008.
[32] L. Onsager, Reciprocal relations in irreversible processes I, Phys. Rev. 37 (1931) 405−426.
[33] J. Ramirez, M. Stan, P. Cristea, Simulations of heat and oxygen diffusion in UO_2 nuclear fuel rods, J. Nucl. Mater. 359 (3) (2006) 174−184, https://doi.org/10.1016/j.jnucmat.2006.08.018.
[34] B. Mihaila, M. Stan, J. Ramirez, A. Zubelewicz, P. Cristea, Simulations of coupled heat transport, oxygen diffusion, and thermal expansion in UO_2 nuclear fuel elements, J. Nucl. Mater. 394 (2−3) (2009) 182−189, https://doi.org/10.1016/j.jnucmat.2009.09.007.

[35] P. Konarski, J. Sercombe, C. Riglet-Martial, L. Noirot, I. Zacharie-Aubrun, K. Hanifi, M. Frégonèse, P. Chantrenne, 3D simulation of a power ramp including fuel thermochemistry and oxygen thermodiffusion, J. Nucl. Mater. 519 (2019) 104–120, https://doi.org/10.1016/j.jnucmat.2019.03.021.
[36] V.D. Ozrin, A model for evolution of oxygen potential and stoichiometry deviation in irradiated UO_2 fuel, J. Nucl. Mater. 419 (1–3) (2011) 371–377, https://doi.org/10.1016/j.jnucmat.2011.06.042.
[37] C. Riglet-Martial, J. Sercombe, J. Lamontagne, J. Noirot, I. Roure, T. Blay, L. Desgranges, Experimental evidence of oxygen thermo-migration in PWR UO_2 fuels during power ramps using in-situ oxido-reduction indicators, J. Nucl. Mater. 480 (2016) 32–39, https://doi.org/10.1016/j.jnucmat.2016.07.056.
[38] R. Niven, B. Noack, Control volume analysis, entropy balance and the entropy production in flow systems, in: R. Dewar, C. Lineweaver, R. Niven, K. Regenauer-Lieb (Eds.), Beyond the Second Law: Entropy Production and Non-equilibrium Systems, Springer-Verlag, 2014, pp. 129–162.
[39] D.R. Gaston, C.J. Permann, J.W. Peterson, A.E. Slaughter, D. Andes, Y. Wang, M.P. Short, D.M. Perez, M.R. Tonks, J. Ortensi, L. Zou, R.C. Martineau, Physics-based multiscale coupling for full core nuclear reactor simulation, Ann. Nucl. Energy 84 (2015) 45–54, https://doi.org/10.1016/j.anucene.2014.09.060.
[40] M. Piro, J. Banfield, K. Clarno, S. Simunovic, T. Besmann, B. Lewis, W. Thompson, Corrigendum to 'Coupled thermochemical, isotopic evolution and heat transfer simulations in highly irradiated UO_2 nuclear fuel', J. Nucl. Mater. 478 (2016) 375–377, https://doi.org/10.1016/j.jnucmat.2016.06.030.
[41] M. Hillert, L. Kjellqvist, H. Mao, M. Selleby, B. Sundman, Parameters in the compound energy formalism for ionic systems, Calphad Comput. Coupling Phase Diagrams Thermochem. 33 (1) (2009) 227–232, https://doi.org/10.1016/j.calphad.2008.05.006.
[42] M. Piro, M. Welland, M. Stan, On the interpretation of chemical potentials computed from equilibrium thermodynamic codes, J. Nucl. Mater. 464 (2015) 48–52, https://doi.org/10.1016/j.jnucmat.2015.04.004.
[43] The Nuclear Energy Agency (NEA), Thermodynamics of Advanced Fuels – International Database (TAF-ID), 2020. https://www.oecd-nea.org/science/taf-id/.
[44] C. Guéneau, S. Gossé, A. Quaini, N. Dupin, B. Sundman, M. Kurata, T. Besmann, P. Turchi, J. Dumas, E. Corcoran, M. Piro, T. Ogata, R. Hania, B. Lee, R. Kennedy, S. Massara, FUELBASE, TAF-ID databases and OC software: advanced computational tools to perform thermodynamic calculations on nuclear fuel materials, in: The 7th European Review Meeting on Severe Accident Research, 2015, pp. 1–10. Marseille, France.
[45] C.W. Bale, E. Belisle, P. Chartrand, S.A. Decterov, G. Eriksson, A.E. Gheribi, K. Hack, I.H. Jung, Y.B. Kang, J. Melancon, A.D. Pelton, S. Petersen, C. Robelin, J. Sangster, P. Spencer, M.A. Van Ende, Factsage thermochemical software and databases, 2010-2016, Calphad Comput. Coupling Phase Diagrams Thermochem. 54 (2016) 35–53, https://doi.org/10.1016/j.calphad.2016.05.002.
[46] M.H. Piro, D. Sunderland, S. Livingstone, J. Sercombe, W. Revie, A. Quastel, K. Terrani, C. Judge, A review of pellet-clad interaction behavior in zirconium alloy fuel cladding, in: Reference Module in Materials Science and Materials Engineering, Elsevier, 2017, pp. 1–68, https://doi.org/10.1016/B978-0-12-803581-8.09799-X.
[47] I. Arimescu, J. Karlsson, Towards understanding beneficial effects of slow power ramps, J. Nucl. Sci. Technol. 52 (10) (2015) 1274–1280.
[48] M. Poschmann, M. Piro, S. Simunovic, Acceleration of Thermochimica Calculations in BISON, Report ORNL/TM-2020/1473, Oak Ridge National Laboratory, 2020.